First Field Measurements of the 15 T Nb₃Sn Dipole Demonstrator MDPCT1

T. Strauss, E. Barzi, J. DiMarco, V.V. Kashikhin, I. Novitski, M. Tartaglia, G. V. Velev, A.V. Zlobin

Abstract—**Within the US Magnet Development Program (MDP), a 15 T Nb₃Sn dipole was developed to demonstrate a possible magnet design for a post-LHC proton-proton Collider. The magnet design is based on 60 mm aperture 4-layer shell-type coils, graded between the inner and outer layers to maximize magnet performance. Magnet coils are surrounded by vertically split thick iron laminations, connected by aluminum I-clamps, and a thick stainless-steel skin. The magnet coils were preloaded to achieve 14 T in the first test. The magnet was tested at the Vertical Magnet Test Facility (VMTF) at Fermilab. This paper reports the first results of magnetic measurements of the 15 T Nb₃Sn dipole demonstrator, including dipole strength, geometrical harmonics, coil magnetization and iron saturation effects. At the maximum quench current of 9742 A we obtained a dipole strength of 14.13 T.**

Index Terms—**Superconducting magnets, Electromagnetic measurements, Accelerator magnets**

I. INTRODUCTION

FERMILAB, in collaboration with members of the US Magnet Development Program (US-MDP), has fabricated and tested a 15 T Nb₃Sn dipole demonstrator suitable for a post-LHC hadron collider [1]. The magnet, called MDPCT1, is based on the optimized "cos-theta" coil design [2],[3]. The main objectives of this magnet are demonstration of the 15 T field level in an aperture suitable for future hadron colliders, and study of the magnet quench performance, critical current, mechanical margins, quench protection, and field quality.

The MDPCT1 design is based on 60 mm aperture 4-layer shell-type coils, using a graded approach between inner and outer layers to maximize magnet performance and minimize the amount of superconductor used. The cable in the two innermost layers has 28 Nb₃Sn RRP strands 1.0 mm in diameter and the cable in the two outermost layers has 40 Nb₃Sn RRP strands 0.7 mm in diameter. A 0.025 mm thick and 11-mm wide stainless-steel core is used in both cables to suppress the interstrand coupling currents induced by the varying magnetic field in coils. The magnet coils are surrounded by vertically split 25.4 mm thick 1020 iron laminations, connected by 7075-T6 aluminum I-clamps, and a 12 mm thick 316 stainless-steel skin. The magnet outer diameter is 612 mm, the length including splice box is 1.46 m, and the mass is 2,390 kg. The

MDPCT1 transverse cross-section with flux lines is displayed in Figure 1 for an aperture field of 13.75 T. The details of magnet design and fabrication, and the quench performance are reported elsewhere [1], [3]. The magnet was tested at the Vertical Magnet Test Facility (VMTF) at Fermilab. For this first test, a preload value calculated for a maximum field of 14 T was chosen to reduce the risk of magnet damage during assembly. This paper presents the results of the MDPCT1 magnetic measurements and includes the dipole strength, geometrical field harmonics, coil magnetization and iron yoke saturation effects, and the normal sextupole decay and snap-back. The results are compared with simulations performed with ROXIE [4] and COMSOL [5] codes.

II. FIELD DEFINITION AND MEASUREMENT SYSTEM

The measured dipole field is expressed in standard form of harmonic coefficients defined in a series expansion of a complex function

$$B_y + iB_x = B_1 10^{-4} \sum_{n=1}^{\infty} (b_n + ia_n)\left(\frac{x+iy}{R_{ref}}\right)^{n-1} \quad (1)$$

where B_x and B_y in (1) are the field components in Cartesian coordinates, b_n and a_n are normal and skew coefficients at the reference radius R_{ref}, normalized to the main field, B_1, and scaled by a factor 10^4 in order to report the harmonics in convenient 'units'. In this analysis, for better comparison, all measurements utilize R_{ref} of 17 mm, which is the nominal value for the LHC dipole magnets. The right-handed measurement coordinate system is defined with the z-axis at the center of the magnet aperture and pointing from return to lead end,
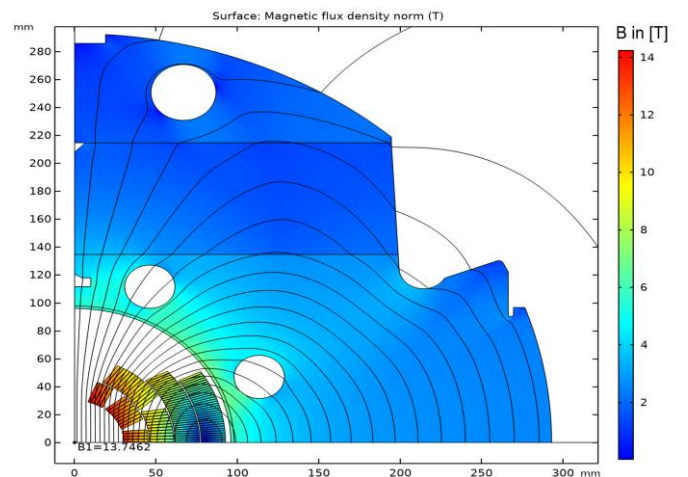

Fig. 1.   Magnetic flux density diagram in the transverse cross-section at $B_{aperture}$=13.746 T.

with z=0 at magnet center. All magnetic measurements were taken at 1.9 K, using a pre-cycle up to 9 kA and down to 0 kA with the ramp rate of 20 A/s followed by: a) a scan of the longitudinal magnet axis at constant current (z-scan) in 22.7 mm increments, b) a ramp profile to 9 kA at varying ramp speed of 20 A/s, 40 A/s and 60 A/s (loop), or c) a stepwise ramp with holding current for 60 seconds up to 9.25 kA (stair step). The simulated accelerator profile consists of a pre-cycle with 10 A/s to 9 kA and a down ramp minimum of 100 A (reset current) and injection plateau at 760 A followed by a 10 A/s ramp to 9 kA.

The rotating coil technique is used to measure field components. The two measurement probes are built on circuit board technology [6] and have a 13 turn, 16-layer PCB pattern with a maximum turn length of 26 mm x 10 mm wide (22.7 mm integrated length, "26 mm probe") and 130 mm x 10 mm wide (126.8 mm integrated length, "130 mm probe") respectively. The latter probe length approximately corresponds to one transposition/twist pitch of the cable. Each probe has a dipole bucked signal to increase measurement accuracy of harmonics. The probe radius of 14 mm was a constraint due to the anti-cryostat diameter used for measurement. It is about 20% smaller than the reference radius $R_{ref.}$

The integration component of the data acquisition system is based on ADC and digital signal processing technology [7]. The system can digitize simultaneously up to 6 channels measuring the magnetic field plus the current signal at a high rotational probe speed. To mitigate the noise from the probes mechanical vibration and to record the voltages from the strong dipole field, rotation speeds between 0.75-1 Hz were used. At these speeds, the combined probe and DAQ sensitivity was estimated to be about 0.1 units for the a_n and b_n harmonics. In these measurements, the standard probe centering using the unallowed sixteen pole was impossible as the a_8 signal was estimated to be below the measurement resolution. However, the estimation of probe centering offset in the magnet body, where loop measurements were made, indicated a value close to zero, as the hysteresis behavior in the normal sextupole showed little sign of feed down to quadrupole.

The bore field measurements with the rotating coils were confirmed using a Metrolab PT2026 device equipped with #1226 NMR probes covering a range of 2.00-5.50 T, and 8.00-22.80 T respectively [8].

III. MEASUREMENT RESULTS AND DISCUSSION

A. Magnet Transfer Function and Strength

Figure 2 shows the measured magnet transfer function ($TF=B_1/I$) versus the magnet current at the longitudinal magnet center. As mentioned previously, two probes with different lengths of 26 mm and 130 mm respectively were used. The magnetic measurements obtained with both probes are identical in the uncertainty estimation, so one representative measurement of the 26 mm probe was chosen to calculate the magnet strength in the high field region. The magnetic measurement system crosscheck with a PT2026 NMR Teslameter [8] showed excellent agreement between the rotating coil and NMR systems within 0.1% or better.
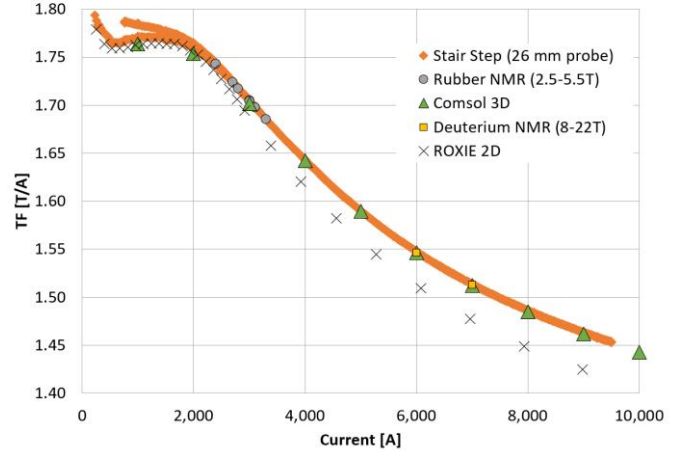

Fig. 2. Measured dipole Transfer Function versus current at the longitudinal magnet center. The rotating coil results are compared with PT2026 NMR measurements, 2D Roxie and 3D COMSOL magnetic field calculations. A 2% discrepancy for high fields in the 2D simulation is expected due to the magnet being relatively short.

To obtain a value for the maximum dipole strength, the *TF* data first were fitted with a linear function in the interval between 9000 and 9500 A. Then the linear fit was extrapolated to the maximum quench current of 9742 A [1], which gave a dipole strength of 14.13 ± 0.02 T.

Figure 2 shows that the 3D COMSOL calculation is in excellent agreement with the measurements, while the 2D ROXIE simulation is up to 2% lower at high currents due to the magnet being relatively short so the higher end field can propagate to the straight section. Due to the proximity of the iron yoke and the coils, the iron saturation effect starts at 2.5 T, see also [9]. The *TF* reduces from 1.778 at low field to 1.452 T/kA at 14 T or 22.5%. At low fields a visible hysteresis in *TF* due to the superconducting coil magnetization is observed.

TABLE I
QUENCH NUMBER, CURRENT AND MEASURED BORE FIELD AND *TF*

Quench Number	Quench Current [A]	Bore Field [T]	*TF* [T/kA]	Temperature [K]
1	7526	11.31	1.503	1.9
2	7598	11.40	1.501	1.9
3	8538	12.61	1.477	1.9
4	9041	13.25	1.466	1.9
5	8944	13.13	1.468	1.9
6	9011	13.21	1.466	1.9
7	9161	13.40	1.463	1.9
8	9360	13.66	1.459	1.9
9	9446	13.76	1.457	1.9
10	9495	13.83	1.456	1.9
11	9517	13.85	1.456	1.9
12	9662	14.04	1.453	1.9
13	9580	13.93	1.454	1.9
14	9690	14.07	1.452	1.9
15	9643	14.01	1.453	1.9
16	9642	14.01	1.453	1.9
17	9705	14.09	1.452	1.9
18	9742	14.13	1.451	4.5

Table I lists the quench numbers, measured quench current and the bore field calculated from a quadratic fit of the stair step measurement bore fields between 7000 A to 9500 A and the previously mentioned linear extrapolation of the maximum quench current bore field. The initial linear fit to extrapolated from 9500 to the maximum quench current was not good to project back to the lower quench current. With this combined method, a small discrepancy to the measurement of 0.02 T between fit and stair step measurement is observed. All the quenches were executed at 1.9 K, except the last quench, which was taken at 4.5 K. The detailed quench performance is
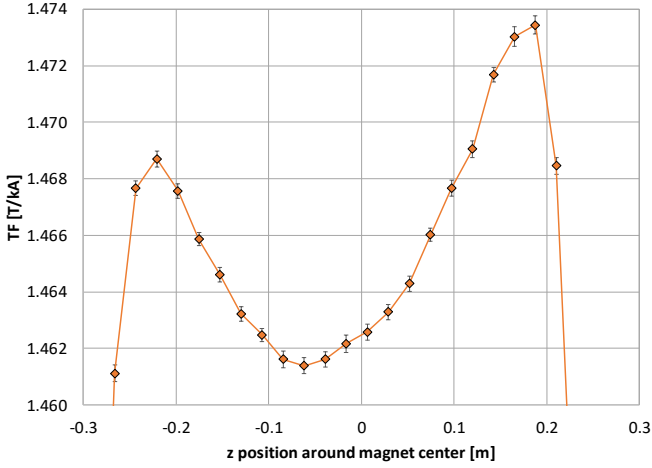

Fig. 3. Transfer Function measured by rotating coil probe along z-axis of the magnet at steady current of 9 kA. The magnet center is selected as zero position.

discussed in [1].

Figure 3 shows axial variation of *TF* at 9 kA, measured using short rotating coil probe. In the magnet end a small (<0.5%) increase of the transfer function is visible, as predicted by the 3D COMSOL simulation.

B. Field Harmonics

Figures 4 show a fine, 22.7 mm step scan of the field harmonics along the magnet z-axis. Except for a_3 and b_3, all the harmonics in the magnet straight section (± 0.2 m) are within ± 5 units. The normal gradient b_2, as well as the normal b_3 and skew a_3 sextupoles change linearly by almost 10 units along the magnet straight section. A 3-unit oscillation over approximately 10 cm, consistent with the 10 cm pitch of the inner cable, is observed in most terms (especially b_5). This could indicate a non-uniform current distribution in the cable cross-section. Similar oscillations of a_2 and b_2 within 3-6 units along the magnet length were also seen in the two-layer 60-mm aperture 11 T dipole models developed at Fermilab for the LHC using similar 40-strand cable and this topic requires further studies [10].

Geometrical harmonics were defined by averaging the measured up-ramp and down-ramp values at 1.5 kA before the iron saturation is in effect. Additional average harmonics measured in a stair step profile are presented in Table II. Above 2.5 T, or above 1.5 kA, the iron saturation effect starts
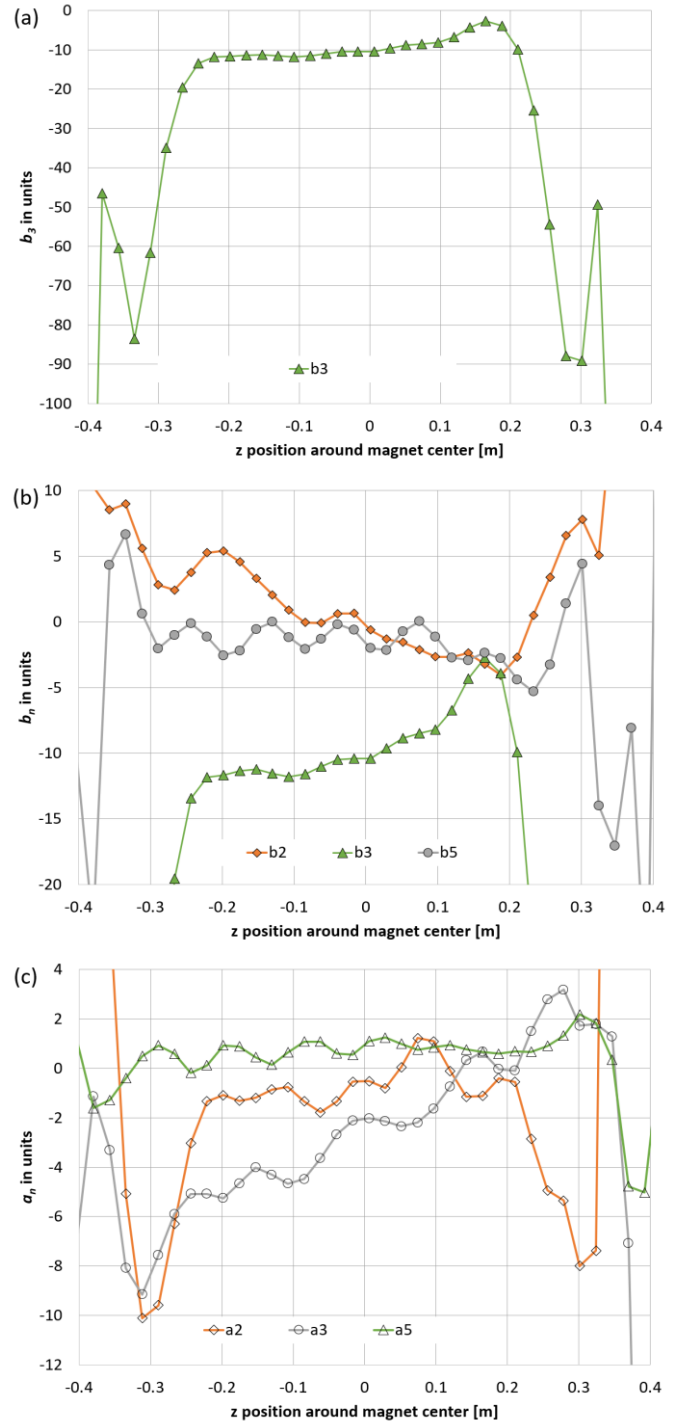

Fig. 4. b_3 (a), normal (b) and skew (c) field harmonics measured by the rotating coil probe along z-axis of the magnet at steady current of 9 kA.

impacting some of the allowed field harmonics during current ramps up and down. All harmonic values for the octupole (n=4) and above, are on the level of 1 unit or less.

The plots in Figure 5 show the hysteresis loop to 9.5 kA at various ramp rates, and the measured dependences of the harmonics versus the main field. The b_3 plot in Figure 5 (a) clearly shows that the influence of the eddy currents inside the strands and the inter-strand coupling currents is minimal (no dependence on the ramp rate), and the large persistent current

effect manifested as a large width of the hysteresis curve. Again, most harmonics are on the order of one unit or less except for the a_3, and b_3, with b_3 as expected from simulations. The a_3 hysteresis is likely due to an asymmetry in coil positions, which generates discrepancy between the field angles of the dipole and the sextupole components. Around 0.9 T the b_3 and b_7 reach a minimum, and b_5 and b_9 have a maximum.

The large hysteresis (persistent current effect), seen at low magnet currents in the TF, b_3 and b_5, is due to the relatively large size of the superconducting filaments and the high critical current density of the Nb_3Sn strands used in this magnet. The iron saturation effect is seen both in TF and b_3. It starts at bore fields above 2.5 T. Both effects are consistent with calculations for the used iron and superconductor magnetization properties and the yoke geometry, as shown in Figures 2 and 6 [9].

C. Sextupole Decay and Snapback

A preliminary look at the normal sextupole field decay and snapback was done, based on the LHC current profile with injection at 760 A and a reset around 100 A. The duration of the injection plateau was fixed at 1800 s and the measurement was taken in the body of the magnet at 1.9 K.

Figure 7 (a) shows the 2-unit decay of b_3 measured with the 26 mm and 130 mm probes. Both measurements were taken simultaneously in the body of the magnet with 130 mm distance between the two probes. The decay and snapback, measured with the 130 mm probe show the same trend as NbTi and Nb_3Sn dipoles measured at Fermilab [11], with a decay amplitude of several units. However, the measurement performed with the 26 mm probe shows an "anomalous", inverse behavior of the decay. Similar anomalous sextupole decay was first observed in the measurements of the Nb_3Sn
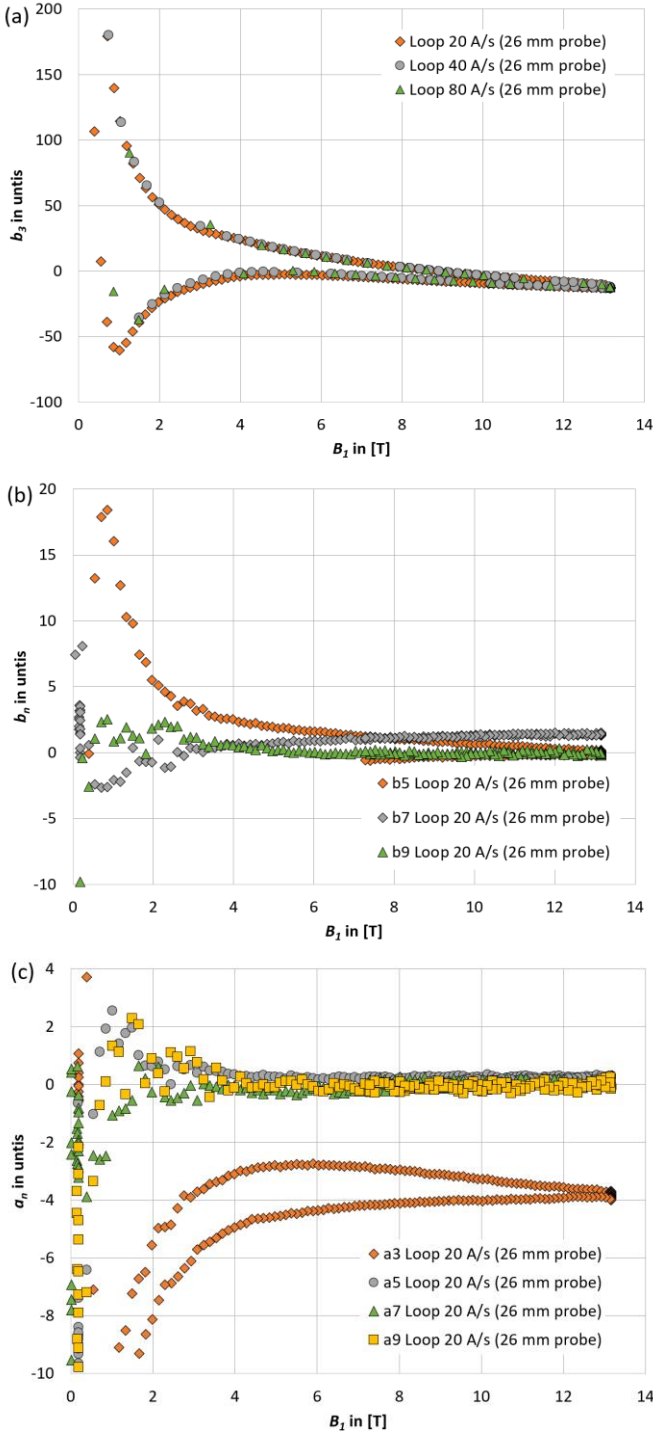

Fig. 5. Harmonic loop measurements to 9 kA at ramp rates of 20 A/s, 40 A/s and 80 A/s. (a) b_3 versus current for all ramp rates, (b) normal harmonics at 20 A/s, and (c) skewed harmonics at 20 A/s.
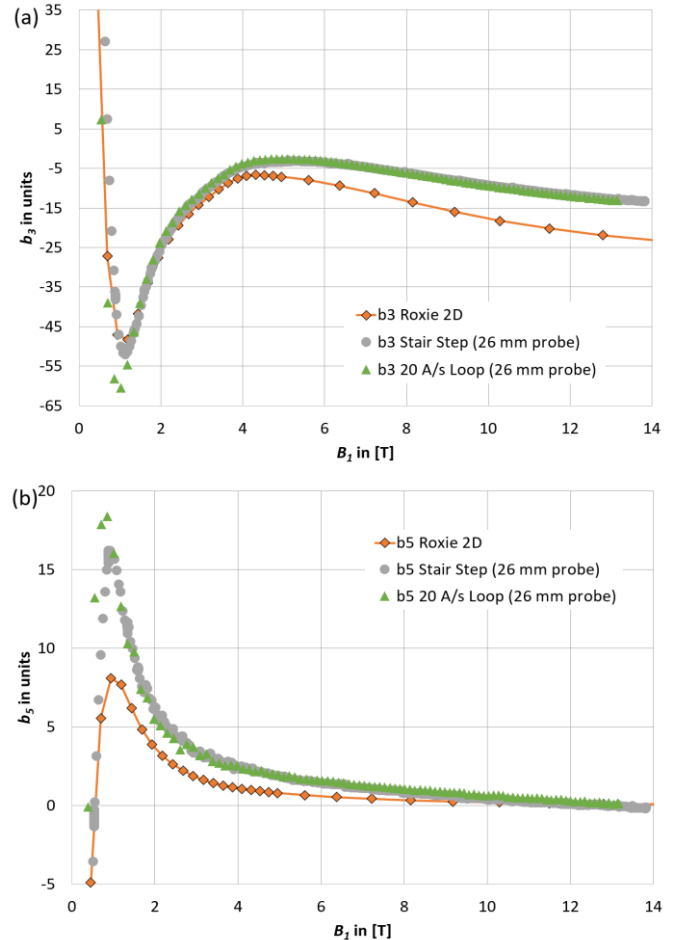

Fig. 6. Calculated and measured (a) b_3, (b) b_5 with coil magnetization and iron saturation effects.

magnets at CERN [12,13], at Fermilab, this behavior is found for the first time.

Figure 7 (b) shows a zoom in time around the snapback, a change of approximately one unit is observed. Some difference in the snapback rates is also seen for the data from
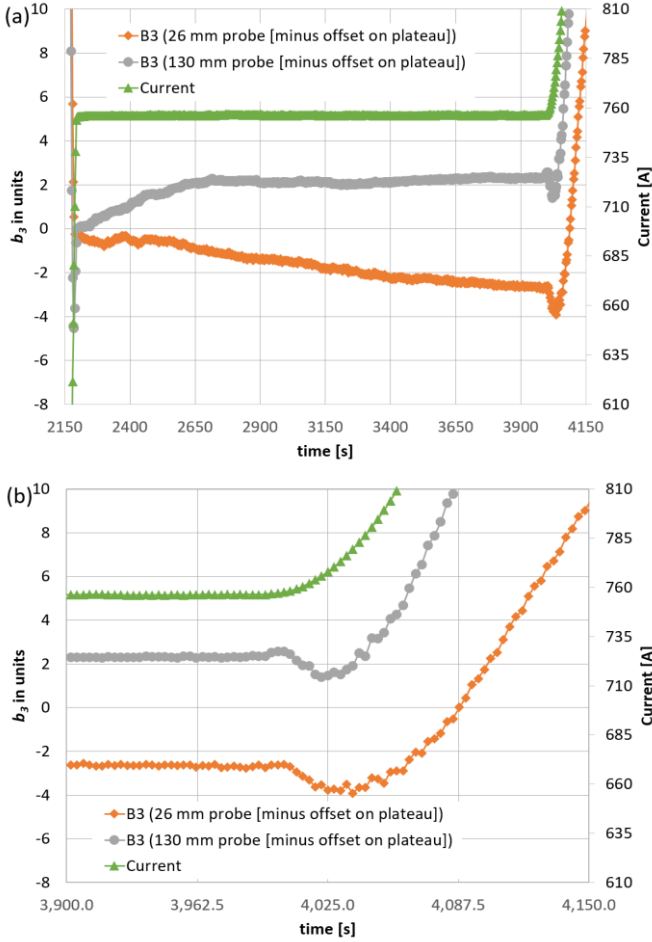

Fig. 7. Decay and snapback in the accelerator current profile: (a) decay plateau, normalized harmonic to initial offset upon reaching plateau, note the decay difference between the 26 mm and 130 mm probes, (b) zoom around the snapback region.

the two probes. Further studies will be required.

IV. CONCLUSION

The dipole field strength and field harmonics were measured for the 15 T Nb$_3$Sn dipole demonstrator MDPCT1 fabricated and tested recently at Fermilab. Based on the measured transfer function, the magnet reached 14.13±0.02 T at 9742 A and 4.5 K – the highest field achieved for accelerator-type magnets at this temperature. By design, the geometrical harmonics in the magnet straight section were minimized optimizing the coil cross-section. Nevertheless, some field harmonics are relatively large due to the deviations of "as-built" coil geometry from the design cross-section. Except for a_2, a_3, b_2, and b_3 the harmonics magnitudes are on the level of 1 unit or less. The large measured iron saturation and coil magnetization effects are consistent with the expectations for this magnet design and cable parameters. Some observed irregularities in the sextupole decay and snapback need more dedicated studies.

ACKNOWLEDGMENT

REFERENCES

[1] A.V. Zlobin et al., "Development and First Test of a 15 T Nb$_3$Sn Dipole Demonstrator MDPCT1", this conference

[2] A.V. Zlobin et al., "Design concept and parameters of a 15 T Nb$_3$Sn dipole demonstrator for a 100 TeV hadron collider", Proceedings of IPAC2015, Richmond, VA, USA, p.3365.

[3] I. Novitski et al., "Development of a 15 T Nb$_3$Sn Accelerator Dipole Demonstrator at Fermilab", IEEE Trans. on Appl. Supercond., Vol. 26, Issue 3, June 2016, 4001007.

[4] ROXIE code for electromagnetic simulations and optimization of accelerator magnets, http://cern.ch/roxie.

[5] COMSOL Multiphysics, https://www.comsol.com.

[6] J. DiMarco et al., "Application of PCB and FDM Technologies to Magnetic Measurement Probe System Development", IEEE Trans. on

TABLE II
AVERAGE HARMONICS

Current [A]	B [T]	TF [T/kA]	b_2	b_3	b_4	b_5	b_6	b_7	b_8	b_9	a_2	a_3	a_4	a_5	a_6	a_7	a_8	a_9
992	1.78	1.793	3.0	13.0	1.1	1.4	0.4	0.6	-0.2	0.3	-3.0	-5.2	-0.6	-0.2	-0.3	-0.1	-0.2	0.5
1492	2.66	1.783	1.9	10.2	0.3	1.0	0.2	0.9	-0.1	0.2	-2.7	-4.1	-0.1	0.0	0.1	0.1	-0.3	0.3
1994	3.53	1.769	1.2	9.5	-0.1	0.7	0.2	1.0	0.0	0.2	-2.0	-3.7	0.1	0.0	0.1	0.1	-0.2	0.2
2494	4.35	1.742	0.8	8.8	-0.4	0.7	0.1	1.0	0.0	0.2	-2.2	-3.5	0.3	0.1	0.1	0.1	-0.1	0.2
2994	5.12	1.709	0.8	6.5	-0.5	0.6	0.1	1.1	0.1	0.2	-2.0	-3.5	0.4	0.1	0.1	0.0	0.0	0.1
3496	5.85	1.673	0.8	4.4	-0.6	0.6	0.1	1.1	0.0	0.1	-1.9	-3.4	0.4	0.0	0.2	0.0	0.0	0.1
3997	6.58	1.645	0.8	2.3	-0.7	0.5	0.0	1.2	0.1	0.1	-1.8	-3.4	0.4	0.1	0.1	-0.1	0.1	0.0
4998	7.95	1.591	1.0	-1.5	-0.8	0.3	0.0	1.2	0.1	0.0	-1.6	-3.4	0.5	0.1	0.1	0.0	0.0	0.0
5997	9.29	1.549	1.2	-4.7	-0.9	0.2	-0.1	1.2	0.1	0.0	-1.4	-3.4	0.6	0.1	0.1	0.0	0.0	0.0
6997	10.60	1.515	1.4	-7.4	-0.9	0.1	-0.1	1.3	0.1	0.1	-1.3	-3.4	0.6	0.1	0.1	0.0	0.0	0.0
7996	11.90	1.487	1.6	-9.6	-1.0	-0.1	-0.1	1.3	0.1	0.1	-1.2	-3.4	0.6	0.2	0.1	0.0	0.0	0.0
8996	13.17	1.465	1.8	-11.5	-1.0	-0.2	-0.2	1.3	0.1	0.1	-1.1	-3.4	0.7	0.2	0.1	0.0	0.0	0.0
9495	13.81	1.454	2.0	-13.2	-1.0	-0.2	-0.2	1.3	0.2	0.1	-1.0	-3.4	0.7	0.2	0.1	0.0	-0.1	0.1

Appl. Supercond., Vol. 23, Issue 3, 2013, p. 9000505.

[7] G.V. Velev et al., "A Fast Continuous Magnetic Field Measurement System Based on Digital Signal Processors", IEEE Trans. of Applied Superconductivity, Vol. 16, No. 2, June 2006, pp. 1374-1377.

[8] The #1226-8.00-22.80 probe was loaned to FNAL by GMW Associates http://www.gmw.com.

[9] V.V. Kashikhin, A.V. Zlobin, "Persistent Current Effect in 15-16 T Nb_3Sn Accelerator Dipoles and its Correction", ISBN 978-3-95450-180-9 Proceedings of NAPAC2016, Chicago, IL, USA, THA1CO04, p. 1061

[10] T. Strauss et al., "Field Quality Measurements in the FNAL twin-aperture 11 T Dipole for LHC Upgrades", ISBN 978-3-95450-180-9 Proceedings of NAPAC2016, Chicago, IL, USA, THA1CO04, p. 158

[11] G. Velev, et al., "Summary of the Persistent Current Effect Measurements in Nb_3Sn and NbTi Accelerator Magnets at Fermilab", IEEE Trans. Appl. Supercond., Vol. 26, No. 4, 2016, Art. 4000605.

[12] S. Izquierdo Bermudez, L. Bottura, L. Fiscarelli, E. Todesco, "Decay and Snapback in Nb_3Sn Dipole Magnets", IEEE Trans. Appl. Supercond., vol. 27, no. 4, 2017, Art. 4002306.

[13] S. Izquierdo Bermude et al., "Magnetic Analysis of the MQXF Qudrupole for the High Luminosity LHC", IEEE Trans. Appl. Supercond., vol. 29, no. 5, 2019, Art. no. 4901705.